Journal of Structural Geology, Vol. 7, No. 1, pp. 73 to 82, 1985
Printed in Great Britain

0191-8141/85 $3.00 + 0.00
Pergamon Press Ltd.

Graphical determination of principal stress directions for slickenside lineation populations: an attempt to modify Arthaud's method

PAWEŁ ALEKSANDROWSKI

Instytut Nauk Geologicznych, Uniwersytet Wrocławski, ul. Cybulskiego 30, 50–205 Wrocław, Poland

(*Received* 23 *September* 1982; *accepted in revised form* 17 *May* 1984)

Abstract—A new method of graphic determination of principal stress directions is proposed for slickenside populations produced in anisotropic rocks. Arthaud's concept of movement planes is advanced through studying variations in their pattern relative to the changing values of the principal stresses. These variations are recognizable by means of a simple test based on the Bott equation. In contrast to Arthaud's method, the proposed procedure is applicable to fault populations resulting from stress fields geometrically reproducible by a triaxial ellipsoid. A field example is given to demonstrate the practical utility of the method.

INTRODUCTION

PRINCIPAL stress directions responsible for faulting in isotropic rocks can be inferred directly from the orientations of fault planes (Anderson 1951). However, most slickenside lineations encountered in the field are those produced in anisotropic rocks. For such media the relationship between the orientations of the principal stresses and the directions of slip on variably oriented pre-existing planes (joints, older faults or bedding surfaces) is more complex, with the magnitude of the intermediate stress σ_2 playing a significant role (Wallace 1951, Bott 1959).

Two graphical methods of analysing slickenside lineation populations have been developed so far. To apply Angelier's method (Angelier 1975, Angelier & Mechler 1977) the sense of movement on each fault examined must be known. This is not the case when employing the method by Arthaud (1969), in which it is sufficient to know the movement sense merely for a part of the slickensides. The Arthaud (1969) method is based on the concept of movement planes. These are the planes perpendicular to fault surfaces and containing the direction of slickenside striae. Applying Arthaud's method to a fault population active in a single tectonic episode, one should:

(1) plot the poles to the fault planes and the penetration points of the striae on a projection net;

(2) join each fault pole and the corresponding striae penetration point with a great circle, thus tracing individual movement planes (M-planes) and

(3) plot the poles (πM-points) to the movement planes.

According to Arthaud (1969), all the M-planes should intersect at one, two or three points that are the axes of the same number of mutually perpendicular great circles of πM-points. The points of intersection of the movement planes correspond to an orthogonal system of deformation axes which determine the directions of maximum shortening (Z), maximum extension (X) and intermediate deformation (Y) of the rock mass under investigation. These axes can be assigned as Z, X or Y according to the sense of relative movement of the fault walls. The axes of deformation are only indirectly related to those of the principal stresses.

Carey (1976) showed that the Arthaud method can be successfully applied only to slickenside lineation populations that originated in radial stress fields (geometrically represented by a uniaxial ellipsoid). The only axis of deformation obtainable from such populations was also proved by her (Carey 1976) to correspond directly to the revolution axis of the stress ellipsoid.

The graphical method proposed here is applicable to a general, triaxial stress state. The method is based on the pattern of behaviour of movement planes recognized while the magnitude ratio between the principal stresses is changing. It may, therefore, be considered as a modification and elaboration of the Arthaud method.

ARRANGEMENT OF MOVEMENT PLANES

In order to study the patterns of movement planes for various relationships between the principal stresses, a simple test was performed. The effects of a few different stress fields on an assemblage of variably oriented planes of anisotropy were simulated by means of computing the directions of maximum shearing stress on these planes, according to the formula derived by Bott (1959)

$$\tan\theta = \frac{n}{lm}\left\{m^2 - (1 - n^2)\frac{\sigma_z - \sigma_x}{\sigma_y - \sigma_x}\right\}, \qquad (1)$$

where θ is the pitch of the maximum shearing stress; l, m and n are the direction cosines of the normal to a slip-plane and σ_x, σ_y and σ_z are the principal stresses parallel to which the co-ordinate axes have been taken. The directions of the maximum shearing stresses were assumed to coincide with those of potential slip-movements (Bott 1959). Bott's formula has been transformed here so that the resulting values are obtained in terms of azimuth and plunge angles of potential fault striae.

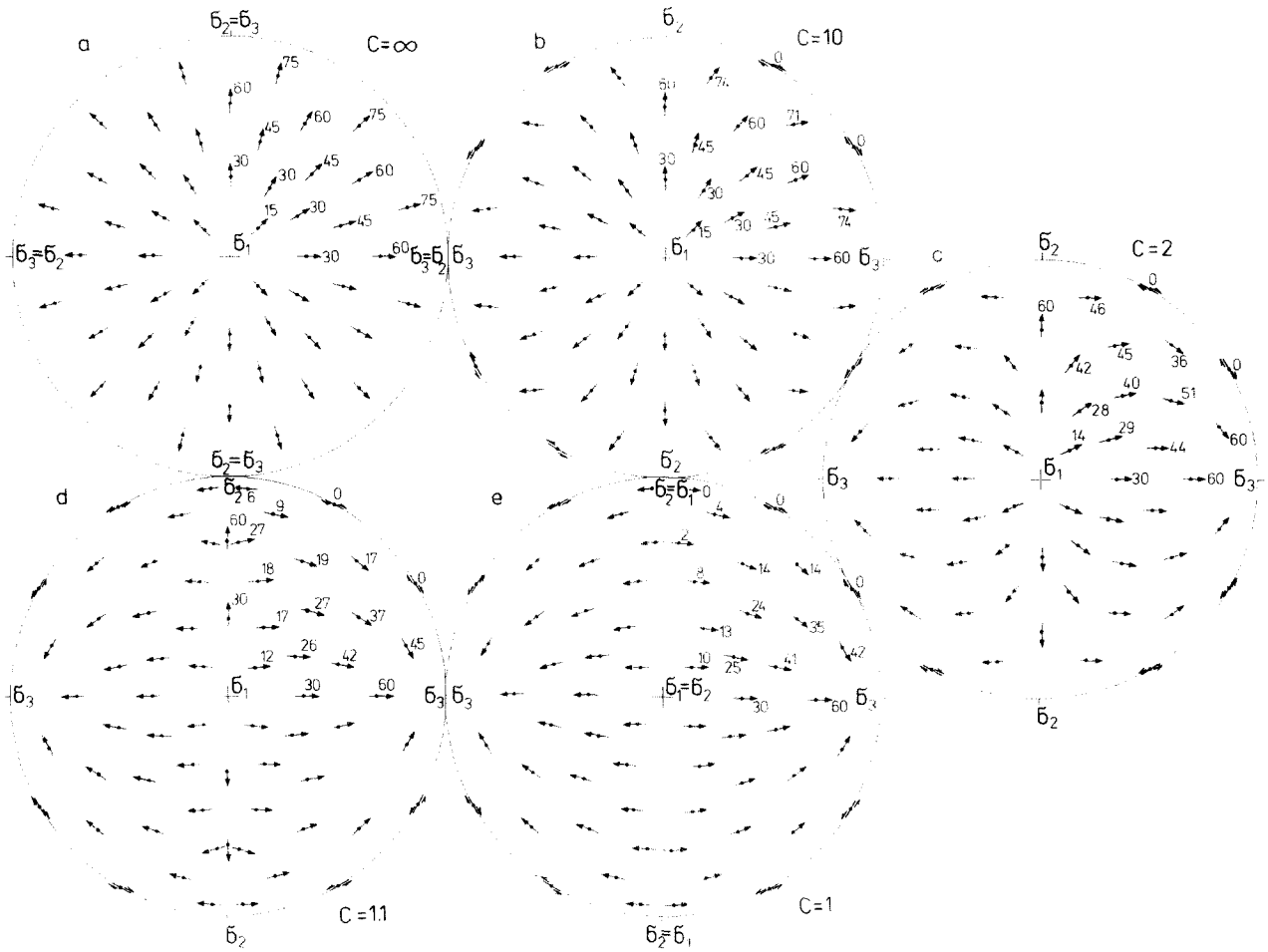

Fig. 1. Slip-movement directions on variably oriented planes for different C values. Arrows are parallel to the azimuths of potential slip-movement (=striae) and indicate the movement sense of 'hanging-walls'. Numbers denote dip angles of striae. Upper-hemisphere equal-area plots are used in this diagram and all subsequent plots. See text for details.

To simplify additional considerations two assumptions are made: (1) the X and Y axes of the co-ordinate system are horizontal with the Y axis facing northwards, while the Z axis is vertical, and (2) $\sigma_z = \sigma_1$, $\sigma_y = \sigma_2$ and $\sigma_x = \sigma_3$, where $\sigma_1 \geq \sigma_2 \geq \sigma_3$ and $\sigma_1 \neq \sigma_3$ (otherwise no shearing stress could exist). Then

$$C = \frac{\sigma_z - \sigma_x}{\sigma_y - \sigma_x} = \frac{\sigma_1 - \sigma_3}{\sigma_2 - \sigma_3}, \qquad (2)$$

where $1 \leq C \leq \infty$, the extreme values of C occurring for $\sigma_1 = \sigma_2$ and $\sigma_2 = \sigma_3$. Both extreme states of stress correspond to radial stress fields.

The computations of potential slip-movement directions were performed for several tens of orientations and for the following C values: $C = \infty$, $C = 10$, $C = 2$, $C = 1.1$ and $C = 1$. The results, which proved to be analogous to those presented by Wallace (1951), are given in Fig. 1. The increasing influence of σ_2 on slip-movement directions with a decrease in C is reflected by the increasing deflection of arrows from the σ_2 position. The computed data were next used for plotting the traces and poles of the movement planes (Fig. 2). The results shown in Figs. 1, 2 and 3 are only those corresponding to particular slip-planes that are arranged along great circles converging at the σ_1, σ_2 or σ_3 points on the diagrams. Such a representation of slip-planes was chosen because of certain specific properties displayed by groups of movement planes, which are related to sets of slip surfaces arranged in this manner (see below).

The patterns of M-planes and πM-points for $C = \infty$ (Fig. 2a) and $C = 1$ (Fig. 2e) clearly confirm the arguments raised by Carey (1976) as to the applicability of Arthaud's method. Namely, in the case of a radial stress tensor all the movement planes have one common intersection point (CIP) which coincides either with the position of σ_1 (for $C = \infty$) or of σ_3 (for $C = 1$). Such an arrangement of M-planes involves the distribution of πM-points along a single great circle (GCP). This GCP is a trace of the plane $\sigma_2\sigma_3$ ($\sigma_2 = \sigma_3$) for $C = \infty$, or of the plane $\sigma_1\sigma_2$ ($\sigma_1 = \sigma_2$) for $C = 1$.

For stress ellipsoids that depart only slightly from the rotative form (e.g. for $C = 10$ and $C = 1.1$) (Figs. 2b & d) this clear picture of the arrangement of M-planes and πM-points becomes partly obliterated. Nevertheless, the majority of CIPs tend to be located close to the position of σ_1 (Fig. 2b) or σ_3 (Fig. 2d), while most πM-points tend to be distributed along the arcs $\sigma_2\sigma_3$ or $\sigma_1\sigma_2$, respectively.

It was also recognized that in the general case of a triaxial stress field (e.g. for $C = 2$) (Fig. 2c) the distribution of movement planes and corresponding π-Mpoints

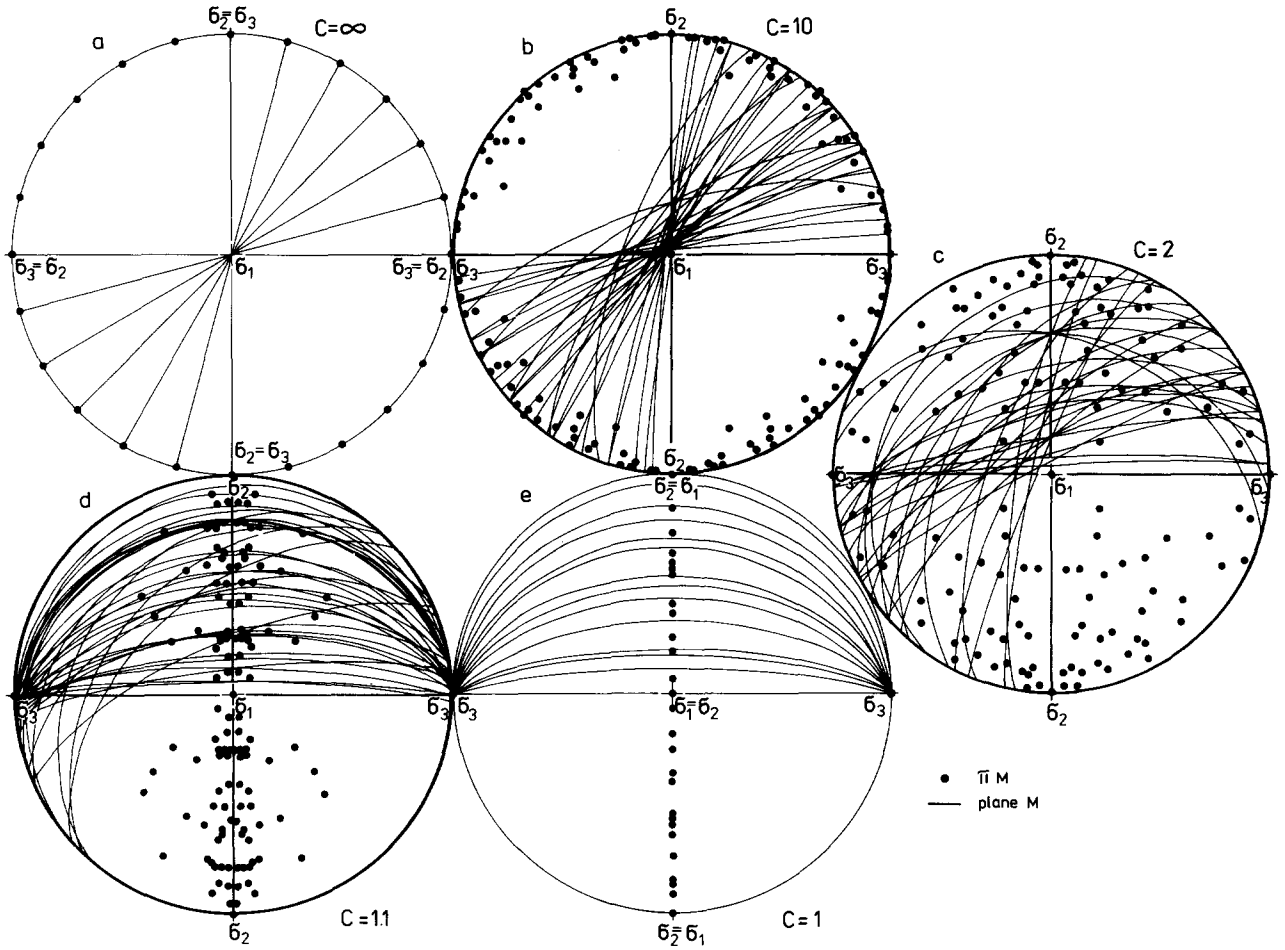

Fig. 2. Patterns of M-planes and πM-points for different C values. Traces of M-planes are plotted only for faults from the 0–90° quarter of the projection circle, whereas πM-points correspond to faults from the whole area of the circle.

continues to be fairly regular. Let us consider in detail the M-plane pattern for the case of $C = 2$ (i.e. when the principal stresses are, for example: $\sigma_1 = 2$, $\sigma_2 = 1$, $\sigma_3 = 0$; or $\sigma_1 = 5$, $\sigma_2 = 1$, $\sigma_3 = -3$; or $\sigma_1 = 6$, $\sigma_2 = 4$, $\sigma_3 = 2$, etc.). It may be inferred from Fig. 3 that if: (a) a group of fault planes is arranged along a great circle and (b) this great circle contains the direction of a principal stress σ, then the movement planes traced for those faults intersect at a CIP located on another great circle perpendicular to the σ position. (From now on the great circles along which fault planes are distributed and which meet requirement (b), will be called GCFs). That is, if a group of slickenside planes is perpendicular to one common plane, and the latter plane is itself parallel to one of the

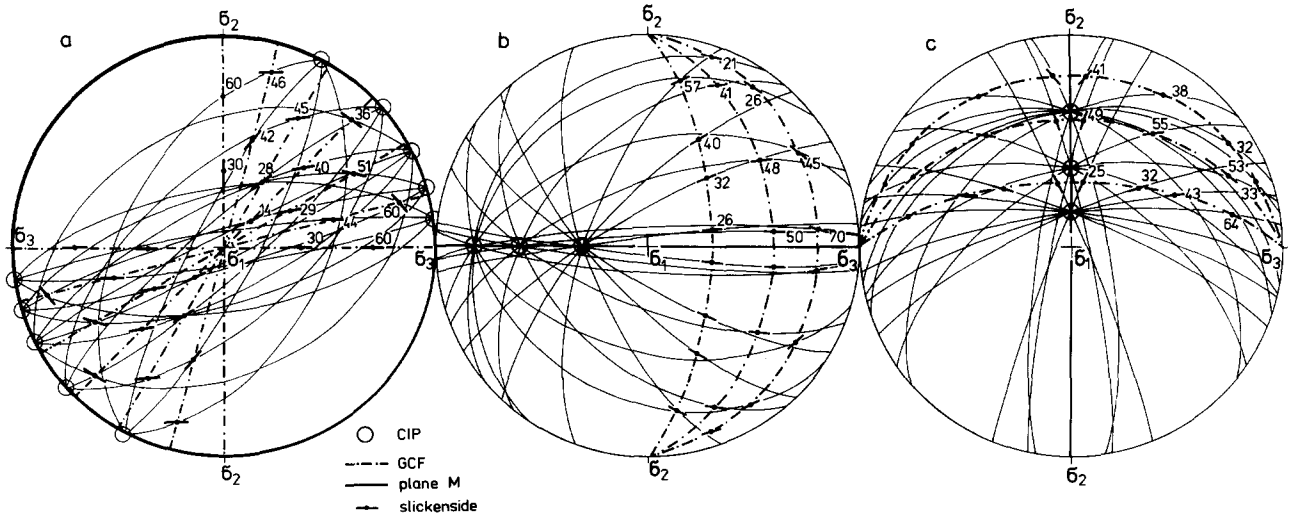

Fig. 3. Movement plane patterns for $C = 2$ drawn separately for groups of slickenside lineations distributed along great circles containing σ_1 (a), σ_2 (b) and σ_3 direction (c).

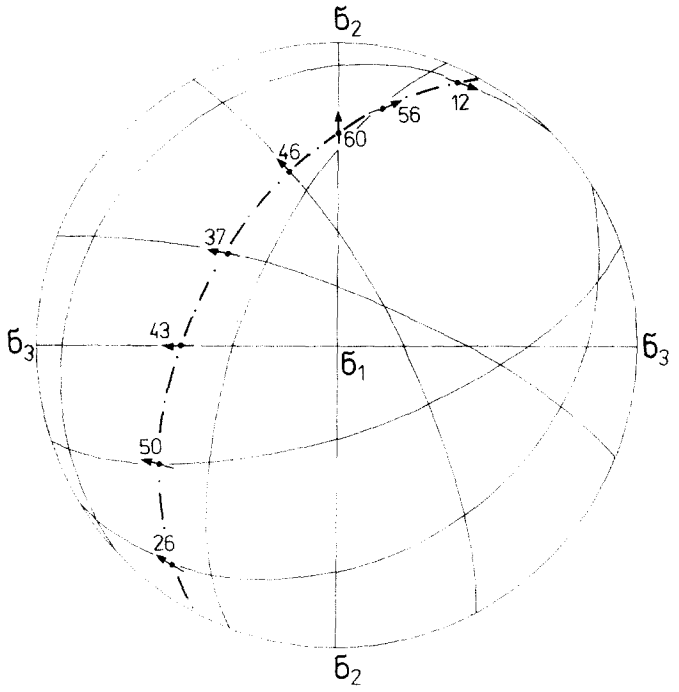

Fig. 4. M-planes pattern for a group of slickenside lineations arranged along a great circle which contains no principal stress direction ($C = 2$).

principal stresses, then all the M-planes related to the slickenside lineations will form a common bundle with a CIP located on the plane which contains the other two directions of principal stress.

In the case under consideration (Fig. 3a), the M-planes traced for slip-surfaces of the same strike (i.e. arranged along a GCF containing the σ_1 direction) intersect at a CIP lying in the $\sigma_2\sigma_3$-plane. For a group of faults of different strike we derive another CIP, but still one which is located in the same $\sigma_2\sigma_3$-plane. If any great circles containing poles to slickensided surfaces converge at the σ_2 point, then all the CIPs for such groups of slickensides are distributed along the trace of the $\sigma_1\sigma_3$-plane (Fig. 3b). Again, for GCFs converging at σ_3, CIPs are arranged along the trace of the $\sigma_1\sigma_2$-plane (Fig. 3c). A similar behaviour of M-planes would also be observable in the cases of $C = 10$ and $C = 1.1$, if the general pattern of arcs shown in Figs. 2(b) & (d) were resolved into three groups, as when $C = 2$.

It should be emphasized that the above principle explaining the arrangement of M-planes can be only applied to those slickenside groups which occupy GCFs, that is the girdles containing the principal stress directions (cf. Fig. 4). Thus any given assemblage of slip-planes constituting a single GCF corresponds to a bundle of M-planes having one CIP. Through this CIP, however, movement planes whose parent slickensides are not arranged along the GCF may fortuitously pass too (cf. Fig. 8c).

From Figs. 2 and 3 it may also be concluded that for a group of slickensides whose normals are located along a GCF, another great circle (GCP) may be defined, composed of πM-poles to the movement planes. Thus, the CIP is an axis of the GCP. Both GCF and GCP girdles intersect at a point corresponding to one of the principal stresses.

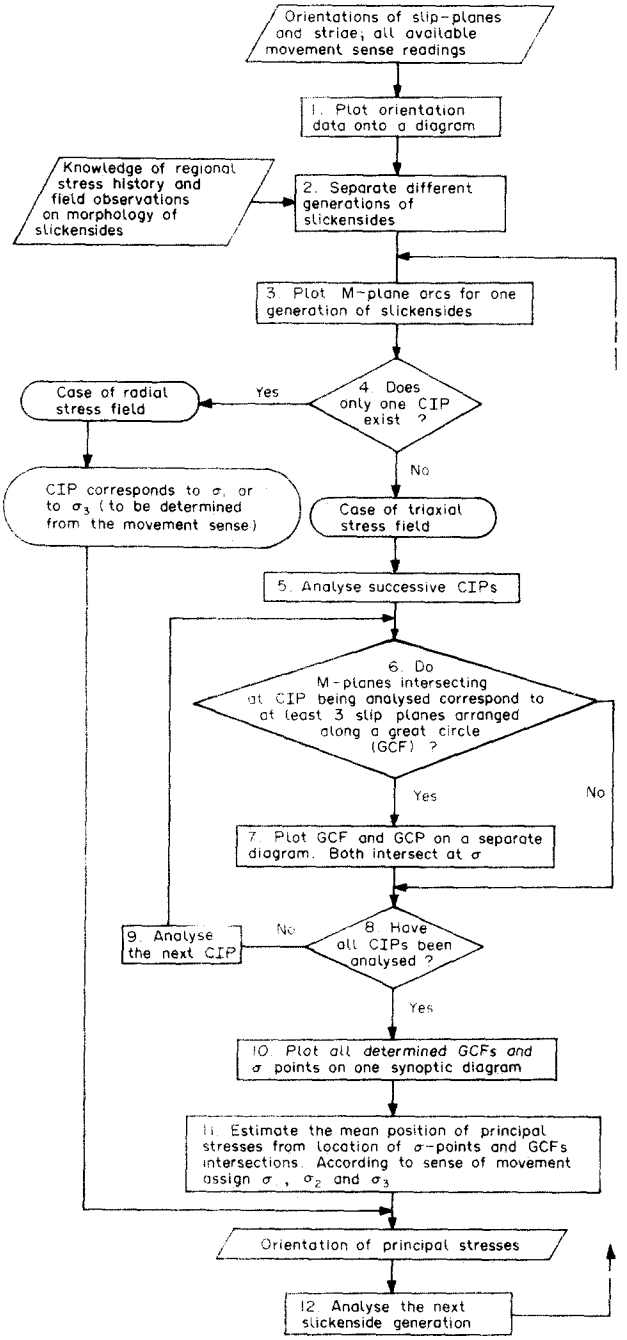

Fig. 5. Sequence of steps in the proposed method.

GRAPHICAL DETERMINATION OF PRINCIPAL STRESS AXES

The above principles may be employed to determine the orientations of the principal stresses of either a radial or a triaxial field responsible for the development of a given fault population. An algorithm of the proposed movement planes method is given in Fig. 5. The following operations require additional comment.

(1) Hoeppener's (1955) method (modified by Jaroszewski 1972) for the presentation of slickenside lineation assemblages is recommended (see Fig. 1).

(2) Orientation data of slickenside lineations resulting from different stress fields are often contradictory. Slickenside lineations that originated in the same stress

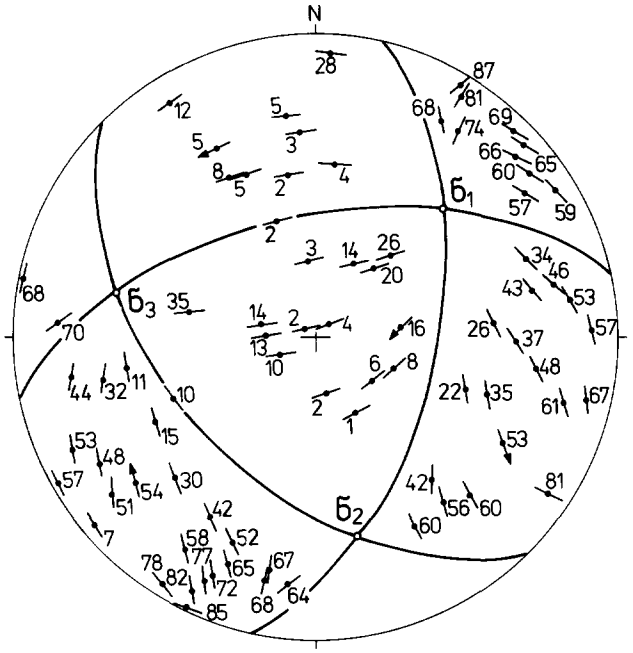

Fig. 6. A theoretical slickenside lineation population. Positions of principal stresses are at first unknown.

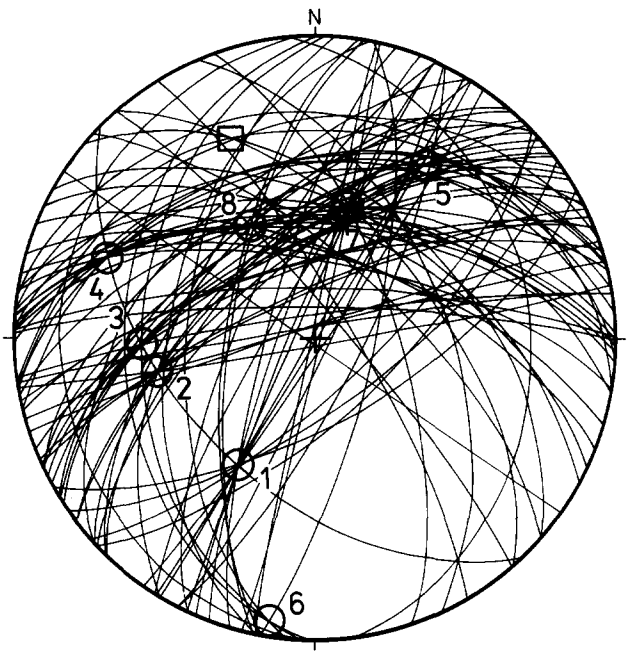

Fig. 7. M-plane pattern corresponding to the slickenside population shown in Fig. 6. Circles and a square indicate CIPs analysed in Fig. 8.

field display patterns similar to those shown in Fig. 1. Field observations of the appearance of slickensides combined with a knowledge of the structural history of a region, should also be taken into account.

(3) M-planes should be plotted as in Arthaud's (1969) method.

(4) Diffuse zones of M-plane intersections plotted from field data may be regarded as CIPs. The positions of the CIPs may be readily determined by plotting πM-points corresponding to single M-plane bundles. The (average) axes of the resulting GCPs are equivalent to the CIPs of the relevant movement planes.

(5) As many as possible CIPs should be separately analysed to check whether or not the slickensides corresponding to the involved movement planes are arranged along great circles (GCFs).

(6) If more than three slickenside planes are distributed (at least roughly) along a GCF, and at large angular distances from each other, the reliability and precision of the solution increase.

It may happen, however, that from the analysis of field data the answer to operation (6) is 'no' for all the CIPs considered. In such a case no solution is likely to be found. Likewise, only one principal stress position may sometimes be arrived at, namely when all the determined σ-points correspond to the same stress axis.

Once the directions of σ_1, σ_2 and σ_3 have been established, it is possible to calculate the C value from the orientation of any slickenside lineation (except for the special case of slip-planes parallel to one of the principal stress directions). To do this, the slickenside orientation should first be found in a co-ordinate system in which the determined σ_1, σ_2 and σ_3 directions follow the X, Y and Z axes, respectively. Thus, the dip direction λ_p and angle of dip ϕ_p of a fault plane are transformed into λ'_p and ϕ'_p, while the trend λ_s and plunge ϕ_s of striations are replaced by λ'_s and ϕ'_s (see Fig. 9). Next, the direction cosines l, m and n of the normal to the slip-plane, as well as the angle θ are computed, using the formulae

$$l = \sin \lambda'_p \sin \phi'_p \tag{3}$$

$$m = \cos \lambda'_p \sin \phi'_p \tag{4}$$

$$n = \cos \phi'_p \tag{5}$$

$$\tan \theta = \frac{\tan (\lambda'_s - \lambda'_p - 90°)}{\cos \phi'_p}. \tag{6}$$

The value of C is derived from Bott's (1959) transformed equation

$$C = \frac{lm}{n - n^3} \left\{ \frac{mn}{l} - \tan \theta \right\}. \tag{7}$$

APPLICATION TO A THEORETICAL EXAMPLE

An artificial, previously calculated ($C = 2$) population of slickenside lineations produced in a triaxial stress field is given in Fig. 6. The arrangement of movement planes (Fig. 7) displays many CIPs at which three or more M-planes intersect. The analysis of the CIPs should reveal those that correspond to slickenside lineations disposed along great circles (GCFs). Eight such CIPs can be found (Fig. 8). When subjected to operation (7) of the algorithm from Fig. 5 the procedure yields σ-points at the intersection sites of (1) GCPs and GCFs and, independently, (2) individual GCFs passing through the same σ-points (Figs. 8a–e). The resultant principal stress axes are shown on a synoptic diagram (Fig. 6), the symbols σ_1, σ_2 and σ_3 being assigned to them on the basis of the known sense of movement on the four faults. Note that the arrows are directed from the σ_1 to the σ_3 point and deflect from the σ_2 position.

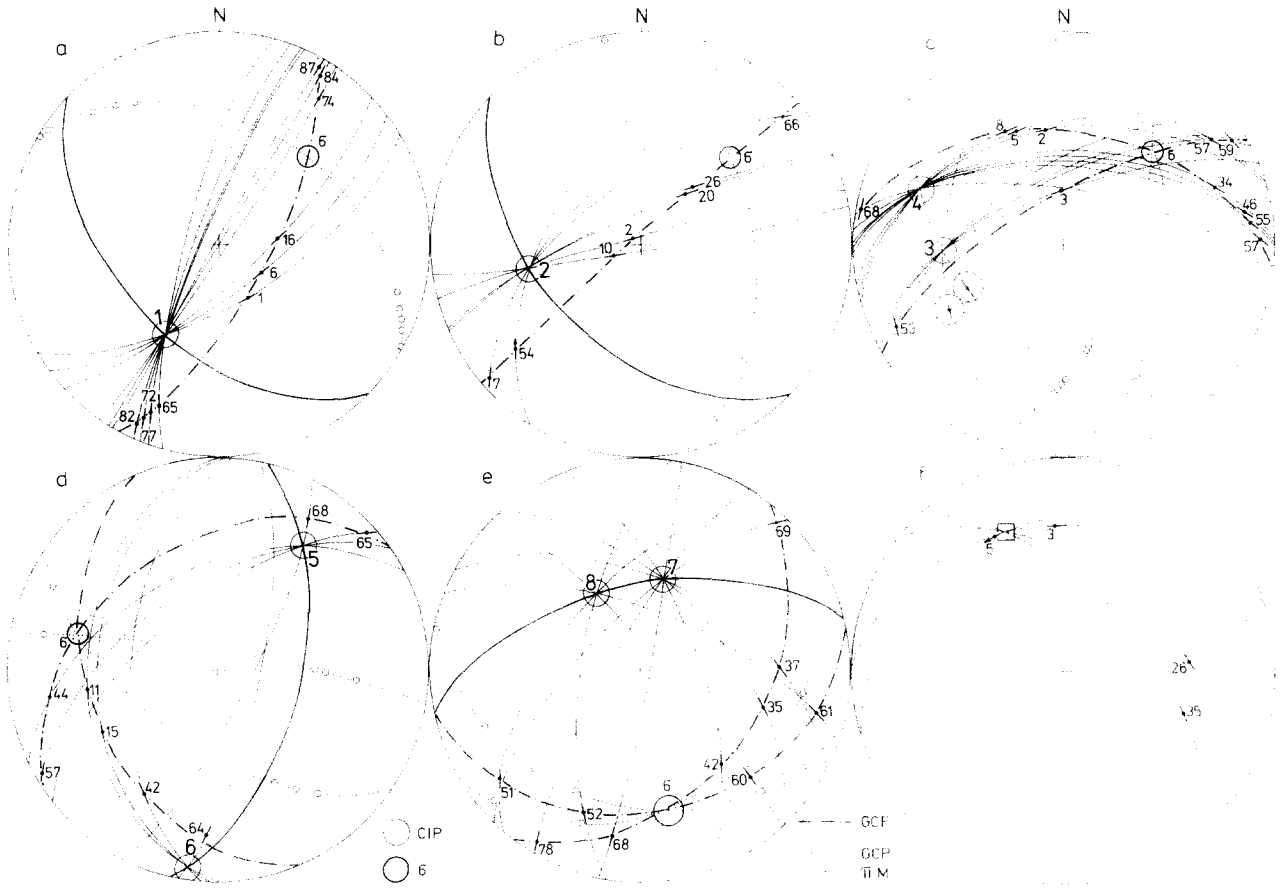

Fig. 8. Individual bundles of M-planes taken from Fig. 7 and analysed separately. Two slickensides (broken circles) which do not pertain to a GCF related to CIP 3, whose M-planes (broken arcs) pass by chance through this CIP, are shown in (c). An example of a 'fortuitous' CIP corresponding to no GCF is given in (f).

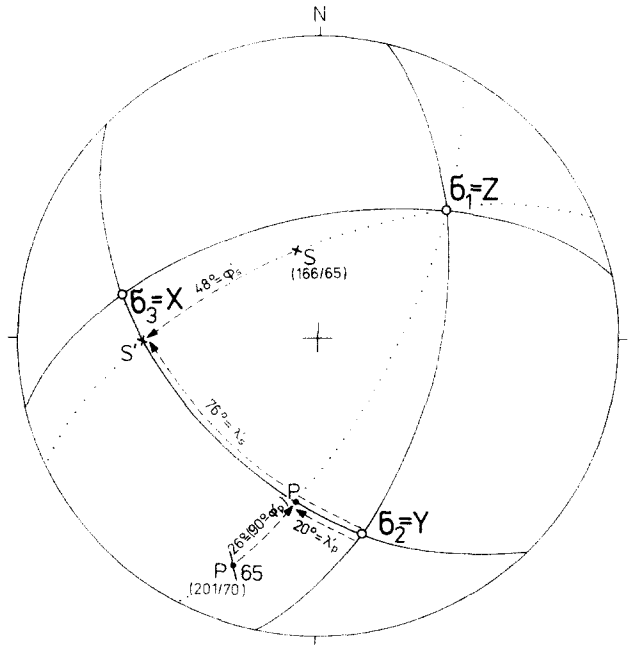

Fig. 9. Transformation of orientation data from the horizontal co-ordinate system into a stress field system (201/70 is the fault-plane dip direction and angle of dip; 166/65 is the striation trend and plunge).

The calculated C value is 2.0 for each slickenside of the population (except one fault located in the $\sigma_2\sigma_3$-plane). The geometric procedure necessary to transform the orientation data is shown in Fig. 9 where slickenside (65) from Fig. 6 serves as an example.

FIELD APPLICATION

The method was tested on several field populations of slickenside lineations from the Outer Carpathians and the Central Sudetes. Positive results were obtained from more than one third of these populations. The validity of the solutions was checked with the Angelier method applied to the same sets of measurements. Moreover, most solutions were independently confirmed by the orientations of a variety of tectonic structures of local and regional significance.

The most instructive of the analysed examples comes from the Mt. Babia Góra region of the Magura nappe of the 'Flysch' Carpathians (Fig. 10). The Magura sequence (Upper Cretaceous to Lower Oligocene) of that region was affected by two main compressive deformation phases (Aleksandrowski 1983). The first occurred in the Early Miocene and resulted in folding and thrusting (Książkiewicz 1977). During this stage 'longitudinal' folds (F_1) developed parallel to the Carpathian chain.

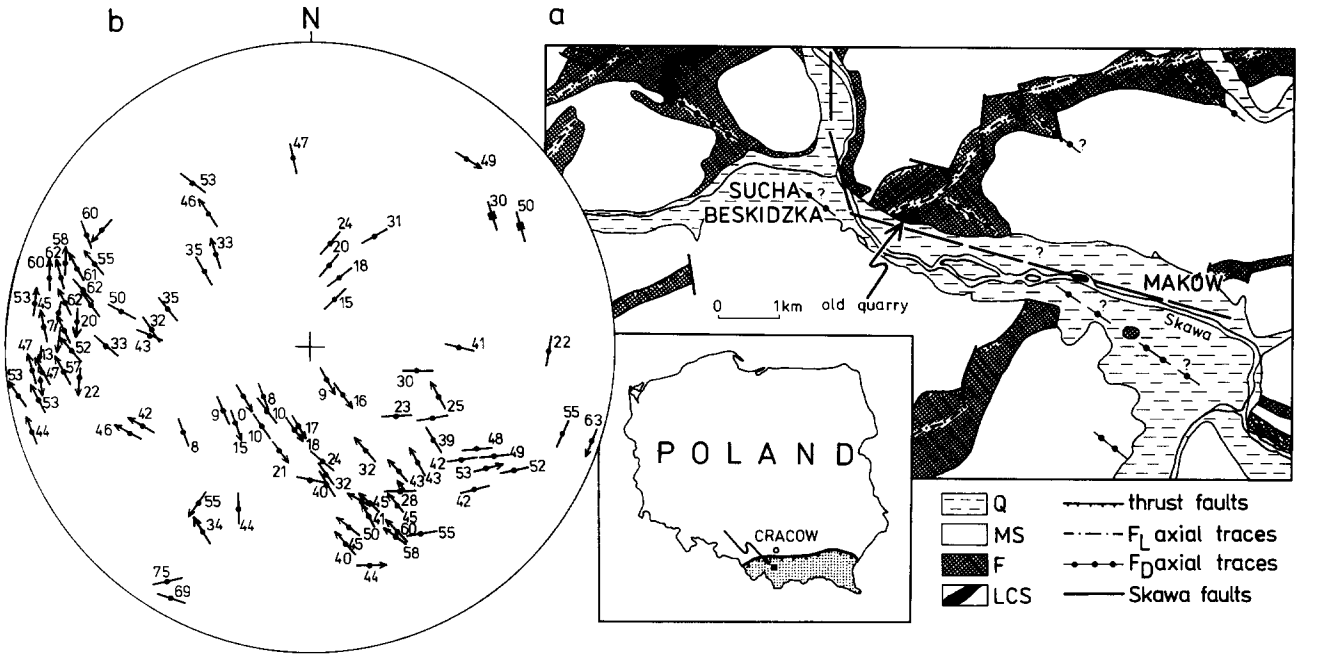

Fig. 10. (a) Location of the investigated outcrop. Q, Quaternary cover; MS, Magura Sandstone; F, flysch members underlying MS; LCS, Lower Ciężkowice Sandstone. (b) Population of slickensides. Strokes with square central points represent faults which fit neither of the two reconstructed stress fields.

The 'diagonal' F_D folds, of NW–SE trend, were produced by the successive, Late Miocene event (Aleksandrowski 1983). The measurements were taken in an abandoned quarry exposing the Lower Ciężkowice Sandstone (Upper Palaeocene), east of Sucha Beskidzka, close to the Skawa river fault. The thick (up to 5 m) sandstone beds dip to the south within a monocline. The beds show a complex joint pattern (Fig. 15). Regionally significant kathetal sets T_1 and T_2 (constituting a complementary system) and set L are genetically related to folds in various parts of the Western Flysch Carpathians (Książkiewicz 1968, Tokarski 1975, Aleksandrowski 1983). Set D, on the other hand, is composed of joints transverse with respect to the F_D folds (Aleksandrowski 1983).

One hundred measured slickenside orientations are shown in Fig. 10(b). Two striae orientation modes are detectable in the diagram, together with a two-fold arrangement of movement planes (Figs. 11a and 12a) permitting almost all the data to be separated into two

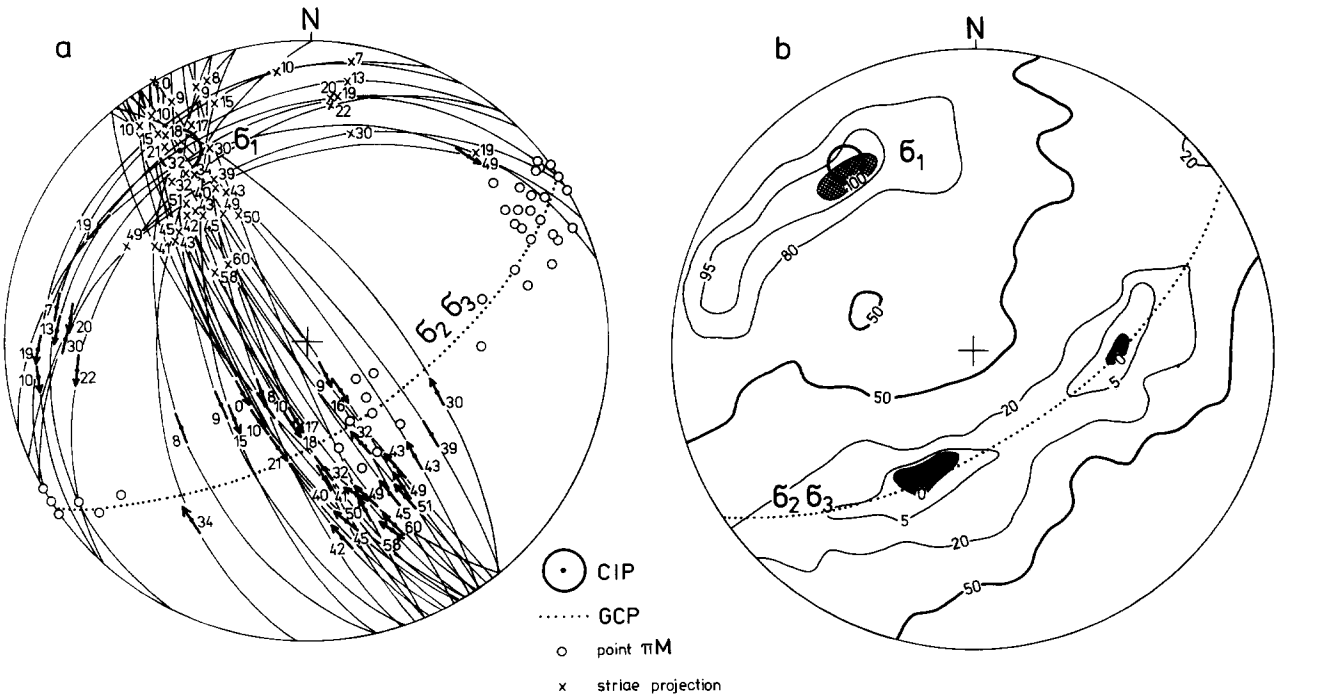

Fig. 11. Group A slickensides. (a) Application of movement planes method. (b) Application of Angelier's method. See text for details.

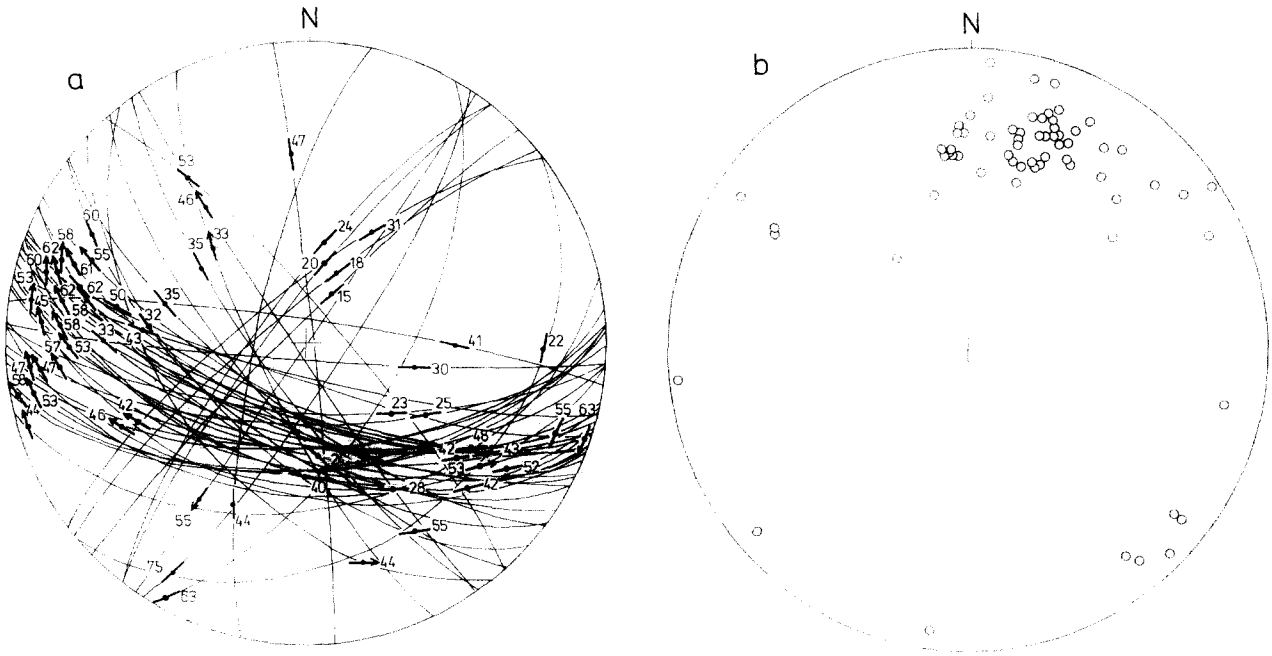

Fig. 12. Group B slickensides. (a) Arrangement of movement planes. (b) Plot of πM-points.

groups. Each of these groups was produced in a different stress field. Movement planes of the first group of slickensides (A) tend to intersect in one common zone (Fig. 11a). Correspondingly, πM-points are arranged along a single great circle. Group A may therefore be interpreted as having originated in a radially compressive stress field (a case to which the classical Arthaud method is applicable). Due to the abundance of faults with known senses of slip, the Angelier construction can also be employed to investigate the group A slickensides. Its application yields the same single maximum corresponding to σ_1 and a diffuse zone of σ_3 positions (Fig. 11b).

The second group (B) of faults (Fig. 12a) resembles in its radial pattern the slickenside arrays illustrated in Figs. 1(c) and 6. The arrows radiate from an empty area (west of the diagram centre); one may expect that this area contains the σ_1 axis. The arrangement of M-planes in addition to the distribution of πM-points (Figs. 12a & b) is irregular and numerous CIPs are present in the diagram. For eight of the CIPs (here zones rather than points) the poles to slip-planes tend to occupy great circles (GCFs) (Fig. 13). This makes it possible to determine the σ_1, σ_2 and σ_3 positions (Fig. 14a). The relatively high dispersion of the location points does not exceed that obtained from Angelier's method (Fig. 14b).

From the data presented in Figs. 10 and 15, it is possible to relate the first, uniaxial stress field (A) to the F_L compressional event. The second of the restored tensors (B), however, shows neither any spatial relationship to the trend of F_D fold axes, nor to joint set D. Apart from the slickenside lineations, the only structures in the outcrop that were probably produced in stress field B are calcite veins up to 1.5 cm thick, designated as V in Fig. 15. The tectonic extension responsible for the development of the group B slickensides must have taken place during one of the post-F_D uplift stages. During the same extensional event the nearby WNW–ESE trending segment of the Skawa river normal fault presumably developed or was reactivated.

Tentative assessments of coefficient C were made for twelve group B faults (Table 1, Fig. 14c). The mean C value calculated for eight examples of slickensides located far from the principal stress planes is 1.99, showing its order of magnitude. At the same time C values assessed for slickensides neighbouring the traces of the $\sigma_1\sigma_2$-, $\sigma_1\sigma_3$- and $\sigma_2\sigma_3$-planes display considerable variations, ranging from 13.34 to -10.38, that is exceeding the admissible lower limit of 1.0 because the orientation of the stress tensor is a mean and not an exact orientation. The inevitable deviations of the natural slickensides from Bott's (1959) equation written for this mean stress tensor orientation, are most severe close to the principal stress planes. Hence the slickensides located in this 'border' zone of the diagram quite often contradict assumptions made to calculate C limits. In a general case C may range between $-\infty$ and $+\infty$ (Armijo *et al.* 1982).

CONCLUSIONS

The proposed method of analysing the arrangement of movement planes supplements the Arthaud method and permits its application to slickenside assemblages resulting from triaxial stress fields. In comparison with Angelier's procedure, the movement planes' method usually gives more precise positions of the stress axes and may be used for investigating minor fault populations with unknown senses of movement reflected by most of the observed slickensides.

There are, however, two considerable disadvantages to the method of movement planes. Firstly, the procedure is time consuming (this may be overcome by using a computer program) and needs many measurements of

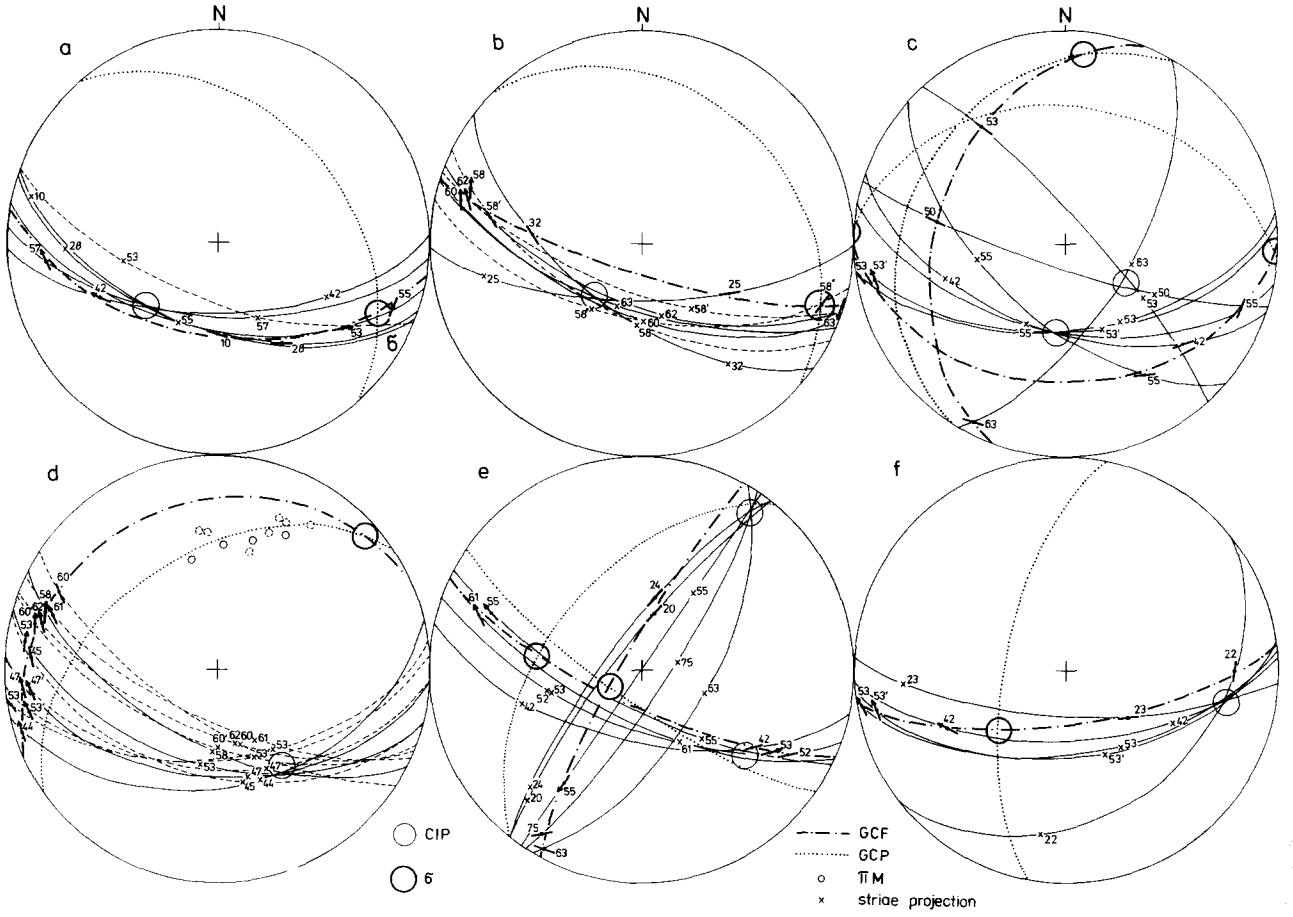

Fig. 13. Determination of principal stress directions for group B slickensides. Shown separately are individual bundles of M-planes corresponding to slip-surfaces arranged along GCFs.

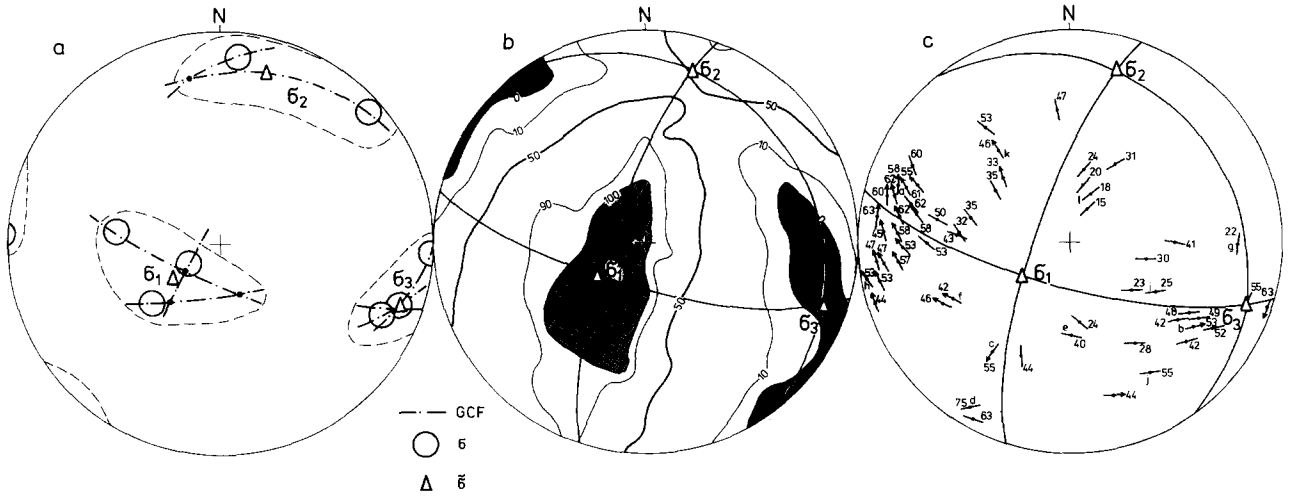

Fig. 14. Results of analysis of group B slickensides. (a) Principal stress axes positions and intersection points of individual GCFs (taken from Fig. 13). Triangles show the mean positions of principal stress axes. (b) Results of application of Angelier's method. Mean positions of stress axes from (a) are shown. (c) Group B slickensides and mean positions of stress axes from (a). Slickensides indicated with letters are those for which C values have been computed.

Table 1. C value calculated for chosen group B slickensides. 'Border' zone slickensides indicated with crosses

Fault symbol in Fig. 14(c)	Coefficient C
a+	−10.38
b+	13.34
c	1.36
d	1.22
e	1.92
f	1.35
g+	−1.36
h	1.77
i+	−0.90
j	3.87
k	1.03
l	3.42

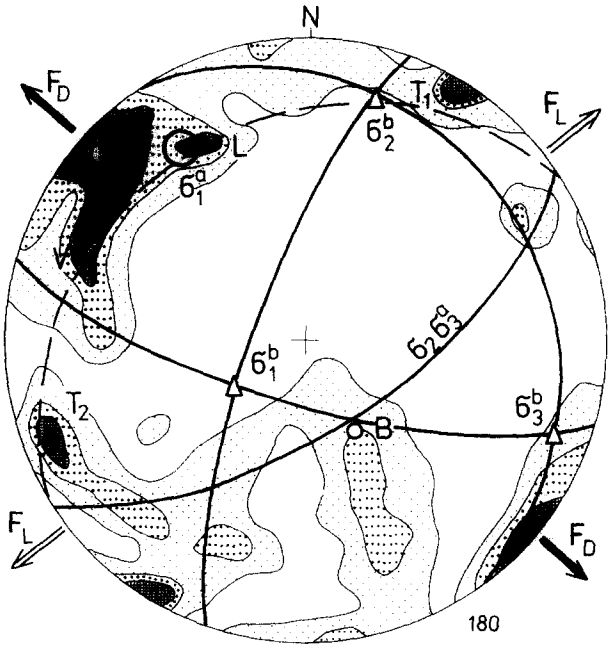

Fig. 15. Joints in the investigated quarry and fold trends from its vicinity. Restored positions of A and B stress tensors are given. Bedding shown as a broken arc (bedding pole = B).

slickenside orientation to be taken; secondly, even a large number of readings does not guarantee a successful result. Moreover, it is not possible to predict before applying the method whether any particular population of data will yield a solution. The resolvability of individual slickenside populations is favoured by a perfectly homogeneous causative stress field, the precision of field measurements and the fulfilment of other necessary conditions, such as no fault-plane rotation during deformation and the independence of movement on each fault (see e.g. Arthaud 1969, Carey 1976, Angelier & Mechler 1977, Armijo *et al.* 1982).

Acknowledgements—I thank Professor W. Jaroszewski and Drs. G. Haczewski, S. J. Porębski, A. K. Tokarski and A. Żelaźniewicz for critically reading the manuscript and offering many valuable suggestions. Debbie Loomis and Paul Hancock helped improve my English and Grażyna Rewus and Andrzej Woch prepared the illustrations.

REFERENCES

Aleksandrowski, P. 1983. A structural analysis of the Magura nappe in the Mt. Babia Góra region, Western Flysch Carpathians. Unpublished Ph.D. thesis (in Polish), Polish Academy of Sciences, Cracow.

Anderson, E. M. 1951. *The Dynamics of Faulting*. Oliver & Boyd, Edinburgh.

Angelier, J. 1975. Sur un apport de l'informatique à l'analyse structurale; exemple de la tectonique cassante. *Revue Géogr. phys. Géol. dyn.* **17**, 137–146.

Angelier, J. & Mechler, P. 1977. Sur une méthode graphique de recherche des contraintes principales également utilisable en tectonique et en séismologie: la méthode des dièdres droits. *Bull. Soc. géol. Fr.*, 7 *Sér.* **19**, 1309–1318.

Armijo, R., Carey, E. & Cisternas, A. 1982. The inverse problem in microtectonics and the separation of tectonic phases. *Tectonophysics* **82**, 145–160.

Arthaud, F. 1969. Méthode de détermination graphique des directions de raccourcissement, d'allongement et intermédiaire d'une population de failles. *Bull. Soc. géol. Fr.*, 7 *Sér.* **11**, 729–737.

Bott, M. H. P. 1959. The mechanics of oblique slip faulting. *Geol. Mag.* **96**, 109–117.

Carey, E. 1976. Analyse numérique d'un modèle mécanique élémentaire appliqué à l'étude d'une population de failles: calcul d'un tenseur moyen des contraintes a partir de stries de glissement. Thèse 3ème cycle. Université de Paris Sud.

Hoeppener, R. 1955. Tektonik im Schiefergebirge. *Geol. Rdsch.* **44**, 26–58.

Jaroszewski, W. 1972. Mesoscopic structural criteria of tectonics of non-orogenic areas: an example from the north-eastern Mesozoic margin of the Świętokrzyskie Mountains. *Studia geol. Polonica* **38**, 1–215.

Książkiewicz, M. 1968. Observations on jointing in the Flysch Carpathians. *Roczn. pol. Tow. geol. (Ann. Soc. géol. Pol.)* **38**, 335–384.

Książkiewicz, M. 1977. The tectonics of the Carpathians. In: *Geology of Poland* (4) *Tectonics* (edited by Pożaryski, W.). Wydawnictwa Geologiczne, Warszawa, 476–620.

Tokarski, A. K. 1975. Structural analysis of the Magura Unit between Krościenko and Zabrzeż (Polish Flysch Carpathians). *Roczn. pol. Tow. geol. (Ann. Soc. géol. Pol.)* **45**, 327–359.

Wallace, R. E. 1951. Geometry of shearing stress and relation to faulting. *J. Geol.* **59**, 118–130.